THE ASTROPHYSICAL JOURNAL, 518:521–532, 1999 June 20

A DEFICIT OF HIGH-REDSHIFT, HIGH-LUMINOSITY X-RAY CLUSTERS: EVIDENCE FOR A HIGH VALUE OF Ω_m?

D. E. REICHART,[1,2] R. C. NICHOL,[2] F. J. CASTANDER,[1] D. J. BURKE,[3]
A. K. ROMER,[2] B. P. HOLDEN,[1] C. A. COLLINS,[3] AND M. P. ULMER[4]
Received 1998 February 9; accepted 1999 January 22

ABSTRACT

From the Press-Schechter mass function and the empirical X-ray cluster luminosity-temperature (L-T) relation, we construct an X-ray cluster luminosity function that can be applied to the growing number of high-redshift, X-ray cluster luminosity catalogs to constrain cosmological parameters. In this paper, we apply this luminosity function to the *Einstein* Medium Sensitivity Survey (EMSS) and the *ROSAT* Brightest Cluster Sample (BCS) luminosity function to constrain the value of Ω_m. In the case of the EMSS, we find a factor of 4–5 fewer X-ray clusters at redshifts above $z = 0.4$ than below this redshift at luminosities above $L_X = 7 \times 10^{44}$ ergs s^{-1} (0.3–3.5 keV), which suggests that the X-ray cluster luminosity function has evolved above $L_\star$. At lower luminosities, this luminosity function evolves only minimally, if at all. Using Bayesian inference, we find that the degree of evolution at high luminosities suggests that $\Omega_m = 0.96^{+0.36}_{-0.32}$, given the best-fit L-T relation of Reichart, Castander, & Nichol. When we account for the uncertainty in how the empirical L-T relation evolves with redshift, we find that $\Omega_m \approx 1.0 \pm 0.4$. However, it is unclear to what degree systematic effects may affect this and similarly obtained results.

Subject headings: cosmology: observation — cosmology: theory — galaxies: clusters: general — galaxies: luminosity function, mass function — X-rays: galaxies

1. INTRODUCTION

The combination of the Press-Schechter mass function (e.g., Press & Schechter 1974; Oukbir & Blanchard 1992; Lacey & Cole 1993) and present and future X-ray cluster catalogs presents a unique opportunity to constrain the cosmological mass density parameter, Ω_m. The Press-Schechter approach offers a number of advantages over various, more traditional methods of measuring this parameter. First of all, numerical simulations reproduce the Press-Schechter mass function to a high degree of accuracy (e.g., Eke et al. 1996; Bryan & Norman 1998; Borgani et al. 1998). Second, unlike methods that only probe Ω_m over small spatial scales—methods that may be insensitive to an underlying, more uniformly distributed component of the dark matter—the Press-Schechter approach probes Ω_m over the scales of X-ray cluster catalogs, which now have limiting redshifts of about unity. Third, the Press-Schechter approach appears to be relatively insensitive to a cosmological constant (e.g., Henry 1997; Mathiesen & Evrard 1998; Eke et al. 1998; Viana & Liddle 1998); consequently, a Press-Schechter–based determination of Ω_m might be compared with independent determinations of the deceleration parameter, for example, to constrain the cosmological constant. Finally and most importantly, a number of independent, high-redshift, X-ray cluster luminosity catalogs with well-understood selection functions are and will soon be available (see § 4). We discuss potential problems with the Press-Schechter approach in § 4.

The archetypal X-ray cluster catalog is the X-ray cluster subsample of the *Einstein* Medium Sensitivity Survey, which we refer to here as the EMSS. A complete description of this sample and its selection criteria can be found in Henry et al. (1992; see also Gioia et al. 1990b; Stocke et al. 1991; Gioia & Luppino 1994). The original EMSS consists of 93 X-ray clusters, of which 67 have redshifts $z \geq 0.14$. Nichol et al. (1997) updated this $z \geq 0.14$ subsample with 21 *ROSAT* luminosities and optical information from the literature. This revised EMSS consists of 64 X-ray clusters, of which 25 have been updated. The redshift and luminosity ranges of the revised EMSS are $0.140 \leq z \leq 0.823$ and 7.5×10^{43} ergs s$^{-1} \leq L_X \leq 2.336 \times 10^{45}$ ergs s^{-1} (0.3–3.5 keV). The EMSS is of great importance because at present it is the only X-ray cluster catalog that probes masses above $M_\star$ at high redshifts, where the Press-Schechter mass function is the most sensitive to Ω_m (see § 3).

Assuming that X-ray clusters correspond to virialized, dark matter halos, the Press-Schechter mass function describes how the X-ray–selected cluster mass function evolves with redshift. Unfortunately, X-ray–selected cluster mass catalogs that span sufficiently broad ranges in M and z to constrain Ω_m do not yet exist. Since the Press-Schechter mass function already assumes that X-ray clusters are virialized, one may convert this mass function to a temperature function with the virial theorem (see § 2); however, X-ray cluster temperature catalogs that span sufficiently broad ranges in T and z to strongly constrain Ω_m also do not yet exist (Viana & Liddle 1998; Blanchard, Bartlett, & Sadat 1998; however, see Henry 1997; Eke et al. 1998). However, several X-ray cluster luminosity catalogs span sufficiently broad ranges in L and z to strongly constrain Ω_m, and the number of such catalogs is growing. However, to fit the Press-Schechter mass function to such catalogs, one must invoke a luminosity-temperature (L-T) relation in addition to the virial theorem. Theoretically, a wide variety of L-T relations have been proposed (e.g., Kaiser 1986; Evrard &

[1] Department of Astronomy and Astrophysics, University of Chicago, 5640 South Ellis Avenue, Chicago, IL 60637.
[2] Department of Physics, Carnegie Mellon University, 5000 Forbes Avenue, Pittsburgh, PA 15213.
[3] Astrophysics Research Institute, Liverpool John Moores University, Liverpool L3 3AF, England, UK.
[4] Department of Physics and Astronomy, Dearborn Observatory, Northwestern University, 2131 Sheridon Road, Evanston, IL 60208.

Henry 1991; Kaiser 1991); consequently, the L-T relation should be determined empirically. Until recently, the L-T relations of temperature catalogs have suffered from much scatter (e.g., Edge & Stewart 1991; David et al. 1993; Mushotzky & Scharf 1997); however, recently Markevitch (1998), Allen & Fabian (1998), and Arnaud & Evrard (1998) have published temperature catalogs with temperatures and luminosities that have either been corrected for or avoided the effects of cooling flows; the result is a significant reduction of this scatter. Using Bayesian inference, Reichart, Castander, & Nichol (1998) have constrained the slope and the evolution of the empirical L-T relation for the luminosity range $10^{44.5}$ ergs s^{-1} $\lesssim L_{\rm bol} \lesssim 10^{46.5}$ ergs s^{-1} and the redshift range $z \lesssim 0.5$ from the Markevitch (1998) and Allen & Fabian (1998) catalogs.

This latter work may be the key to determining cosmological parameters with X-ray cluster catalogs: given a well-constrained L-T relation, the Press-Schechter mass function may be fitted to the growing number of independent, high-redshift, high-luminosity X-ray cluster catalogs with well-understood selection functions. Using the cooling flow–corrected L-T relation of Reichart et al. (1998), we do this to the EMSS and the *ROSAT* Brightest Cluster Sample (BCS) luminosity function of Ebeling et al. (1997) in § 3. In § 2 we model the X-ray cluster luminosity function; in § 4 we draw conclusions and discuss future applications of this luminosity function to the Southern Serendipitous High-Redshift Archival *ROSAT* Catalog (SHARC) and the Bright SHARC.

2. THE MODEL

2.1. *The X-Ray Cluster Luminosity Function*

Assuming that X-ray clusters correspond to virialized, dark matter halos, we model the comoving number density of X-ray clusters with the Press-Schechter mass function, which is given by (e.g., Lacey & Cole 1993)

$$\frac{dn_c(M, z)}{dM} = -\sqrt{\frac{2}{\pi}}\,\frac{\bar{\rho}_0}{M^2}\,\frac{d\ln\sigma_0(M)}{d\ln M}\,\frac{\delta_{c0}(z)}{\sigma_0(M)} \times \exp\left[\frac{-\delta_{c0}^2(z)}{2\sigma_0^2(M)}\right], \quad (1)$$

where $n_c(M, z)$ is the comoving number density of X-ray clusters of mass M at redshift z, $\delta_{c0}(z)$ is the present linear theory overdensity of perturbations that collapsed and virialized at redshift z, $\sigma_0(M)$ is the present linear theory variance of the mass density fluctuation power spectrum filtered on mass scale M, and $\bar{\rho}_0$ is the present mean mass density of the universe. In the case of zero cosmological constant, which we assume throughout this paper, the present overdensity is given by (Lacey & Cole 1993; Peebles 1980)

$$\delta_{c0}(z) = \begin{cases} \frac{3}{2}\,D(0)\left[\left(\frac{2\pi}{\sinh\eta-\eta}\right)^{2/3}+1\right] & (\Omega_m<1), \\ \frac{3}{20}\,(12\pi)^{2/3}(1+z) & (\Omega_m=1), \\ \frac{3}{2}\,D(0)\left[\left(\frac{2\pi}{\eta-\sin\eta}\right)^{2/3}-1\right] & (\Omega_m>1), \end{cases} \quad (2)$$

where

$$D(0) = \begin{cases} 1+\frac{3}{x_0}+\frac{3\sqrt{1+x_0}}{x_0^{3/2}}\ln\left(\sqrt{1+x_0}-\sqrt{x_0}\right) & (\Omega_m<1), \\ -1+\frac{3}{x_0}-\frac{3\sqrt{1+x_0}}{x_0^{3/2}}\tan^{-1}\sqrt{\frac{x_0}{1-x_0}} & (\Omega_m>1), \end{cases} \quad (3)$$

$$x_0 = |\,\Omega_m^{-1}-1\,|\,, \quad (4)$$

$$\eta = \begin{cases} \cosh^{-1}\left[\frac{2}{\Omega(z)}-1\right] & (\Omega_m<1), \\ \cos^{-1}\left[1-\frac{2}{\Omega(z)}\right] & (\Omega_m>1), \end{cases} \quad (5)$$

$$\Omega(z) = \frac{\Omega_m(1+z)}{1+\Omega_m z}\,. \quad (6)$$

We assume a scale-free mass density fluctuation power spectrum of power law index n, so the present variance is given by (e.g., Lacey & Cole 1993)

$$\sigma_0(M) = \sigma_8\left(\frac{M}{M_8}\right)^{-(3+n)/6}, \quad (7)$$

where σ_8 is the amplitude of the mass density fluctuation power spectrum over spheres of radius 8 h^{-1} Mpc and M_8 is the mean mass within these spheres.

We now convert equation (1) from a mass function to an appropriately defined luminosity function. Following the notation of Mathiesen & Evrard (1998), we begin by assuming that X-ray clusters' bolometric luminosities scale as power laws in mass and redshift:

$$L_{\rm bol} \propto M^p(1+z)^s\,. \quad (8)$$

As did Henry et al. (1992) in the case of the EMSS, we find that the fractions of this luminosity that fall into the EMSS band of 0.3–3.5 keV and the BCS band of 0.1–2.4 keV are well approximated by power laws in X-ray cluster temperature:

$$L_{\rm X} = f_{\rm X}\,T^{-\beta}L_{\rm bol}\,, \quad (9)$$

where $f_{\rm X} = 0.989 \pm 0.014$ and $\beta = 0.407 \pm 0.008$ for the representative temperature range of the EMSS ($3 \lesssim T \lesssim 10$ keV) and $f_{\rm X} = 1.033 \pm 0.012$ and $\beta = 0.472 \pm 0.008$ for the representative temperature range of the BCS ($1.5 \lesssim T \lesssim 12$ keV), where temperature is measured in keV. At lower temperatures, however, these approximations quickly fail. Equation (9) is independent of redshift because X-ray cluster luminosities are measured in the source frame. The temperature dependence introduced by equation (9) is removed with the virial theorem:

$$T \propto M^{2/3}(1+z)\,. \quad (10)$$

Technically, this expression holds only when $\Omega_m = 1$; however, we show in § 4 that generalizing this expression has little effect on our results. Together, equations (8), (9), and (10) yield the following expression that relates an X-ray cluster's mass to its observed luminosity, $L_{\rm X}$:

$$L_{\rm X} \propto f_{\rm X}\,M^{p-2\beta/3}(1+z)^{s-\beta}\,. \quad (11)$$

Substitution of equation (11) into equation (1) yields the following luminosity function:

$$\frac{dn_c(L_X, z)}{dL_X} = f(z)L_X^{-1-[(3-n)/2(3p-2\beta)]} \times \exp\left[-g(z)L_X^{(3+n)/(3p-2\beta)}\right], \quad (12)$$

where

$$f(z) = af_X^{[(3-n)/2(3p-2\beta)]}(1+z)^{[(s-\beta)(3-n)]/2(3p-2\beta)}\delta_{c0}(z), \quad (13)$$

$$g(z) = cf_X^{-(3+n)/(3p-2\beta)}(1+z)^{-[(s-\beta)(3+n)]/3p-2\beta}\delta_{c0}^2(z), \quad (14)$$

and a and c depend on σ_8 and the factor of proportionality of equation (11). Instead of trying to model this factor of proportionality and fitting to σ_8, we simply fit to such degenerate, or grouped, combinations of these parameters in this paper (see § 2.2).

Since luminosities are computed from measured fluxes and redshifts, L_X is a function of H_0 and Ω_m. With one exception, all dependences on H_0 can be grouped into the parameters a and c, and this exception is noted in § 2.2. The EMSS and the BCS provide luminosities in their respective X-ray bands that have been computed for $H_0 = 50$ km s^{-1} Mpc^{-1} and $\Omega_m = 1$; we denote these luminosities by L_1. The relationship between L_X and L_1 is given by

$$L_X = x(z)L_1, \quad (15)$$

where

$$x(z) = \begin{cases} \left[\dfrac{d_L(\Omega_m)}{d_L(\Omega_m = 1)}\right]^2 \dfrac{f_F[d_A(\Omega_m = 1)]}{f_F[d_A(\Omega_m)]} & (Einstein) \\ \left[\dfrac{d_L(\Omega_m)}{d_L(\Omega_m = 1)}\right]^2 & (ROSAT), \end{cases} \quad (16)$$

$d_L(\Omega_m)$ is luminosity distance, $d_A(\Omega_m)$ is angular diameter distance, and $f_F[d_A(\Omega_m)]$ is the fraction of an X-ray cluster's flux that is detected in the 2.'4 × 2.'4 detect cell of the original EMSS.[5] A complete description of this quantity can be found in Henry et al. (1992). Since *ROSAT* measures total fluxes, $f_F[d_A(\Omega_m)] = 1$ here. So in the case of the BCS, the latter expression applies. However, the revised EMSS subsample that we fit to in § 3.3 is a combination of 43 *Einstein* luminosities and 18 *ROSAT* luminosities (see § 3). Fortunately, 36 of the 43 *Einstein* clusters have redshifts of $z < 0.33$, and six of the remaining seven clusters have redshifts of $z < 0.47$. At these redshifts, the ratio of fractional fluxes in the former expression for $x(z)$ is within a few percent of unity for a wide range of values of Ω_m. Furthermore, *ROSAT* luminosities are available for seven of the eight clusters that carry the majority of the weight in the fits of § 3.3, and the remaining *Einstein* cluster is at a redshift of $z = 0.259$. Consequently, we also use the latter expression for $x(z)$ in the case of the EMSS. Besides, we show in § 3 that the sensitivity of $x(z)$ to Ω_m plays only a tertiary role in the determination of this parameter. Substitution of equation (15) into equation (12) allows the luminosity function to be fitted to L_1 data without loss of generality:

$$\frac{dn_c(L_1, z)}{dL_1} = f(z)L_1^{-1-[(3-n)/2(3p-2\beta)]} \times \exp\left[-g(z)L_1^{(3+n)/(3p-2\beta)}\right], \quad (17)$$

where

$$f(z) = af_X^{(3-n)/2(3p-2\beta)}(1+z)^{[(s-\beta)(3-n)]/2(3p-2\beta)} \times \delta_{c0}(z)x^{-[(3-n)/2(3p-2\beta)]}(z), \quad (18)$$

$$g(z) = cf_X^{-[(3+n)/(3p-2\beta)]}(1+z)^{-[(s-\beta)(3+n)/(3p-2\beta)]} \times \delta_{c0}^2(z)x^{(3+n)/(3p-2\beta)}(z). \quad (19)$$

2.2. *The Selection Function*

Let $A(L_1, z)$ be the area of the sky that an X-ray survey samples at redshift z as a function of luminosity L_1. In the case of the EMSS, this quantity is given by (Avni & Bahcall 1980; Henry et al. 1992; Nichol et al. 1997)

$$A(L_1, z) = A[F_{lim} = F(L_1, z)], \quad (20)$$

where $A(F_{lim})$ is the area of the sky that the EMSS surveyed below sensitivity limit F_{lim} (see Henry et al. 1992),

$$F(L_1, z) = \frac{f_F[d_A(z)]}{k(z)} \frac{h_{50}^2 L_1}{4\pi d_L^2(z)}, \quad (21)$$

and $k(z)$ is the k-correction from the observer frame to the source frame for a $T = 6$ keV X-ray cluster; the exact dependence of $k(z)$ on X-ray cluster temperature can be ignored for the representative temperature range of the EMSS. For the EMSS, we have computed $A(L_1, z)$ for 41 values of L_1 between $10^{43.5}$ and $10^{45.5}$ ergs s^{-1} (0.3–3.5 keV) and for $\Omega_m = 0$, 0.5, 1, and 1.5. For intermediate values of L_1 and Ω_m, we use linear interpolation between $43.5 < \log L_1 < 45.5$ and $0 < \Omega_m < 1.5$. The cases of $\Omega_m = 0$ and 1 are plotted in Figure 1. The dependence of $A(L_1, z)$ on H_0 cannot be grouped into the parameters a and c, unlike all of the other H_0 dependences in this analysis (§ 2.1). Instead of making H_0 a free parameter, we fix $H_0 = 50$ km s^{-1} Mpc^{-1}

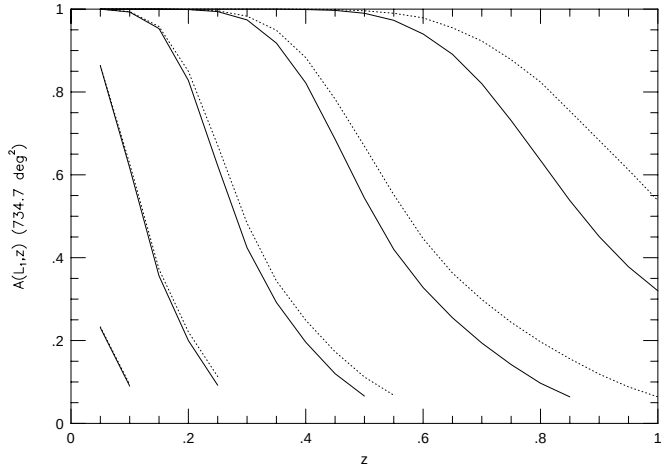

FIG. 1.—Area $A(L_1, z)$ of the sky that the EMSS sampled at redshift z as a function of luminosity L_1. The solid curve is for $\Omega_m = 0$, and the dotted curve is for $\Omega_m = 1$. From left to right, the curves correspond to $L_1 = 10^{43.5}$, 10^{44}, $10^{44.5}$, 10^{45}, and $10^{45.5}$ ergs s^{-1} (0.3–3.5 keV) (see § 2.2).

[5] The quantity $f_F[d_A(\Omega_m)]$ is also a function of X-ray cluster core radius, a_0, which Henry et al. (1992) found to be $a_0 \sim 0.25$ Mpc, assuming that $\Omega_m = 1$. Repeating their analysis for $\Omega_m = 0$, we find that this result again holds; consequently, we adopt this value of a_0 throughout this paper.

in this paper. However, if others wish to be more general, they need only consider the H_0 dependence of the selection function. The case of the BCS is treated separately in § 3.2.

The total number of X-ray clusters observed between luminosity and redshift limits $L_l < L_1 < L_u$ and $z_l < z < z_u$, i.e., the cumulative luminosity function, is given by

$$N(L_l, L_u; z_l, z_u) = \int_{L_l}^{L_u} \int_{z_l}^{z_u} A(L_1, z) \frac{dn_c(L_1, z)}{dL_1} dL_1 \, dV(z) , \tag{22}$$

where

$$dV(z) = \frac{4c^3 dz}{H_0^3 \Omega_m^4 (1+z)^3} \times \frac{(\Omega_m z + (\Omega_m - 2)[(\Omega_m z + 1)^{1/2} - 1)]^2}{(1+\Omega_m z)^{1/2}} \tag{23}$$

is the comoving volume element. Hence, our model (luminosity function + selection function) consists of nine parameters: $H_0, f_X, \beta, p, s, a, c, n$, and Ω_m. We have fixed the value of H_0, and we have tightly constrained the values of f_X and β for the EMSS and the BCS (§ 2.1). In § 3.1 we adopt values of p and s from the Bayesian inference analysis of the X-ray cluster L-T relation of Reichart et al. (1998), and in § 3.3, the normalization parameter, a, drops out of the Bayesian inference analysis of this paper. This leaves three parameters: Ω_m, n, and the grouped parameter c, which depends on σ_8, the proportionality constant of equation (11), and H_0. We determine credible intervals for the values of these three parameters in § 3.3.

3. BAYESIAN INFERENCE

If properly applied, equation (22) can be an effective probe of Ω_m. In this cumulative luminosity function, $\delta_{c0}(z)$, $A(L_1, z)$, $x(z)$, and $dV(z)$ depend on Ω_m. We now consider how sensitive each of these quantities is to Ω_m. The comoving volume element $dV(z)$ is approximately given by (eq. [23])

$$\frac{dV(z)}{dz} \propto \begin{cases} \dfrac{z^{2.26}}{(1+z)^3} & (\Omega_m = 0) \\ \dfrac{z^{1.99}}{(1+z)^3} & (\Omega_m = 1) , \end{cases} \tag{24}$$

where the indices apply in the redshift range $0.14 < z < 0.6$. The luminosity conversion expression, $x(z)$, is approximately given by (eq. [16])

$$x(z) \approx 1 - \frac{1-\Omega_m}{4} z , \tag{25}$$

and in equation (17), it is always raised to a power that is between ≈ -1.5 and ≈ 0.5. Consequently, $dV(z)$ and $x(z)$ contribute only weak dependences on Ω_m to equation (22). The present overdensity is a stronger function of Ω_m (eq. [2]):

$$\delta_{c0}(z) = \begin{cases} 1.5 & (\Omega_m = 0) \\ 1.69(1+z) & (\Omega_m = 1) , \end{cases} \tag{26}$$

Since this expression appears to the second power in the exponential cutoff of equation (17), it contributes a significant dependence on Ω_m to the cumulative luminosity function. For example, if the luminosity function is observed to cut off prematurely at higher redshifts, i.e., if there is a deficit of high-redshift, luminous X-ray clusters, then higher values of Ω_m are favored. However, if little or no evolution is manifest in the observed X-ray cluster luminosity function, particularly above $L_\star$,[6] then lower values of Ω_m are favored.

The surveyed area, $A(L_1, z)$, contributes a different type of dependence on Ω_m to the cumulative luminosity function. In the case of the EMSS (see Fig. 1), this dependence is negligible at low luminosities and redshifts. However, at luminosities $\gtrsim L_\star$, $A(L_1, z)$ is a nonnegligible, increasing function of Ω_m at sufficiently high redshifts. For example, in the case of an $L_1 = 10^{45}$ ergs s^{-1}, $z = 0.8$ EMSS cluster, $A(L_1, z)$ is roughly twice as large in an $\Omega_m = 1$ universe than it is in an $\Omega_m = 0$ universe. Although this effect is suppressed by the exponential cutoff of equation (17) above $L_\star$, this effect is amplified about $L_\star$ by the fact that the luminosity function itself is a nonnegligible, increasing function of Ω_m at luminosities $\lesssim L_\star$ at these high redshifts (see § 3.3). Consequently, we find that an overabundance of high-redshift, $\sim L_\star$ EMSS clusters favors higher values of Ω_m and not lower values of this parameter as is generally thought. We return to this idea in § 3.3.

Consider first the case of X-ray cluster luminosity data that lie within a narrow redshift band of effective redshift $z_{\rm eff}$. Then, up to a factor of $A(L_1, z_{\rm eff}) dV(z_{\rm eff})/dz$, the integrand of equation (22) (eq. [17]) is simply a power law in luminosity with an Ω_m-dependent exponential cutoff. This exponential cutoff is a function of the parameters f_X, β, p, n, and $g_{\rm eff} = g(z_{\rm eff})$, which itself is a function of Ω_m (see below). We have already constrained the values of f_X and β (§ 2.1), and we adopt the Reichart et al. (1998) value of p, as well as that of s, in § 3.1. However, there are too few high-luminosity X-ray clusters to simultaneously constrain n and $g_{\rm eff}$. Fortunately, n is also constrained by the low-luminosity, power-law limit of equation (17) for which data are more plentiful. Consequently, by fitting this luminosity function to data of this type, n and $g_{\rm eff}$ can be jointly constrained.

By equation (19), the parameter $g_{\rm eff}$ is a function of $z_{\rm eff}$ and of the parameters f_X, β, p, s, n, c, and Ω_m. The effective redshift is a given, and the parameters f_X, β, p, s, and n can be constrained as described above. However, since $z \approx z_{\rm eff}$, a constant, the parameters c and Ω_m are degenerate; consequently, Ω_m can only be constrained if the value of c is otherwise known, i.e., if the values of σ_8, the factor of proportionality of equation (11), and H_0 are otherwise known (§ 2.2). Even in the event that X-ray cluster mass data are used instead of luminosity data, any fitted value of Ω_m will still depend strongly on the assumed value of σ_8, as well as on the assumed value of n, since mass data are not yet plentiful enough for the Press-Schechter mass function to constrain these parameters.

However, now consider X-ray cluster luminosity data that span a breadth of redshifts. Instead of constraining the single parameter $g_{\rm eff}$, one instead constrains a distribution of such parameters with redshift, i.e., $g(z)$. The normalization of this distribution is c, and its shape yields Ω_m since the parameters f_X, β, p, s, and n are otherwise constrained. Consequently, by fitting equation (22) to the EMSS, which spans a breadth of luminosities and redshifts, the param-

[6] In this paper, $L_\star$ refers very generally to those luminosities at which the luminosity function, modeled by equation (17), appears to roll over from a power law to an exponential cutoff.

eters n, c, and Ω_m can be jointly constrained regardless of the values of σ_8 and the factor of proportionality of equation (11) [but not regardless of the value of H_0 since $A(L_1, z)$ is a function of this parameter (§ 2.2)]. We do this for the EMSS in § 3.3. In § 3.2 we better constrain the parameters n and c (actually, $g_{\rm eff}$) with the local ($z_{\rm eff} \sim 0.1$) luminosity function of the BCS. First however, we discuss the cooling flow–corrected L-T relation of Reichart et al. (1998) and its implied values of p and s in § 3.1.

3.1. *The L-T Relation*

The combination of equations (8) and (10) yields the L-T relation:

$$L_{\rm bol} \propto T^{3p/2}(1+z)^{s-(3p/2)} . \quad (27)$$

Reichart et al. (1998) have constrained the slope and the evolution of equation (27) using the cooling flow–corrected X-ray cluster temperature catalogs of Markevitch (1998) and Allen & Fabian (1998) and Bayesian inference. For the luminosity ranges of the EMSS and the BCS, and the redshift range $z \lesssim 0.5$, they find that $p = 1.86^{+0.10}_{-0.10}$ and $s = (3.77 - 0.63\Omega_m)^{+0.48}_{-1.22}$. However, when using the L-T relation to fit the Press-Schechter mass function to X-ray cluster luminosity catalogs (1) that are not cooling flow corrected and (2) for which X-ray cluster photon count rates have been converted to fluxes and luminosities by assuming a $T = 6$ keV thermal bremsstrahlung spectrum, they find that one should use $p = 1.77^{+0.16}_{-0.13}$ and $s = (3.14 - 0.65\Omega_m)^{+0.88}_{-0.86}$.

In the case of the EMSS, this latter case applies. In this paper, we adopt the best-fit values: $p = 1.77$ and $s = 3.14 - 0.65\Omega_m$. The parameter p is well constrained, and in § 3.3 we show that the uncertainty in the value of s does not significantly affect our results. In the case of the BCS, luminosities are not cooling flow corrected, but they are not determined by assuming $T = 6$ keV for each X-ray cluster; instead, luminosities are determined by additionally requiring that each X-ray cluster satisfy an L-T relation (Ebeling et al. 1997). From Figure 1 of Reichart et al. (1998), it is apparent that the assumption of $T = 6$ keV more strongly affects the value of p than does the use of cooling flow–corrected luminosities. Consequently, in this paper, we adopt $p = 1.86$ in the case of the BCS. We note, however, that such minor variations in this parameter do not significantly affect our results. Since the BCS is a local ($z_{\rm eff} \sim 0.1$) catalog, the value of s is unimportant in this case (see § 3.2).

3.2. *The ROSAT BCS*

The *ROSAT* BCS is a flux-limited sample of 199 bright X-ray clusters. A complete description of this sample and its selection criteria can be found in Ebeling et al. (1997). The redshift range of the BCS is $z < 0.3$; however, most of the BCS clusters have redshifts of $z < 0.2$, and the effective redshift (see § 3) of the sample is $z_{\rm eff} \sim 0.1$. Consequently, the BCS samples the X-ray cluster population of the local universe. Although such a sample may not have enough redshift leverage to adequately probe Ω_m, its large size makes it an excellent sample to constrain the parameters n and c (actually, $g_{\rm eff}$; § 3). These constraints can then be combined with the EMSS results of § 3.3 to better constrain Ω_m. However, since the BCS is not yet publicly available, we settle here for a simplified analysis of the binned BCS luminosity function of Figure 1 of Ebeling et al. (1997), which we replot in Figure 2.

Since the BCS spans a relatively narrow band of redshifts, we let $f(z) = f(z_{\rm eff}) = f_{\rm eff}$ and $g(z) = g(z_{\rm eff}) = g_{\rm eff}$ in equa-

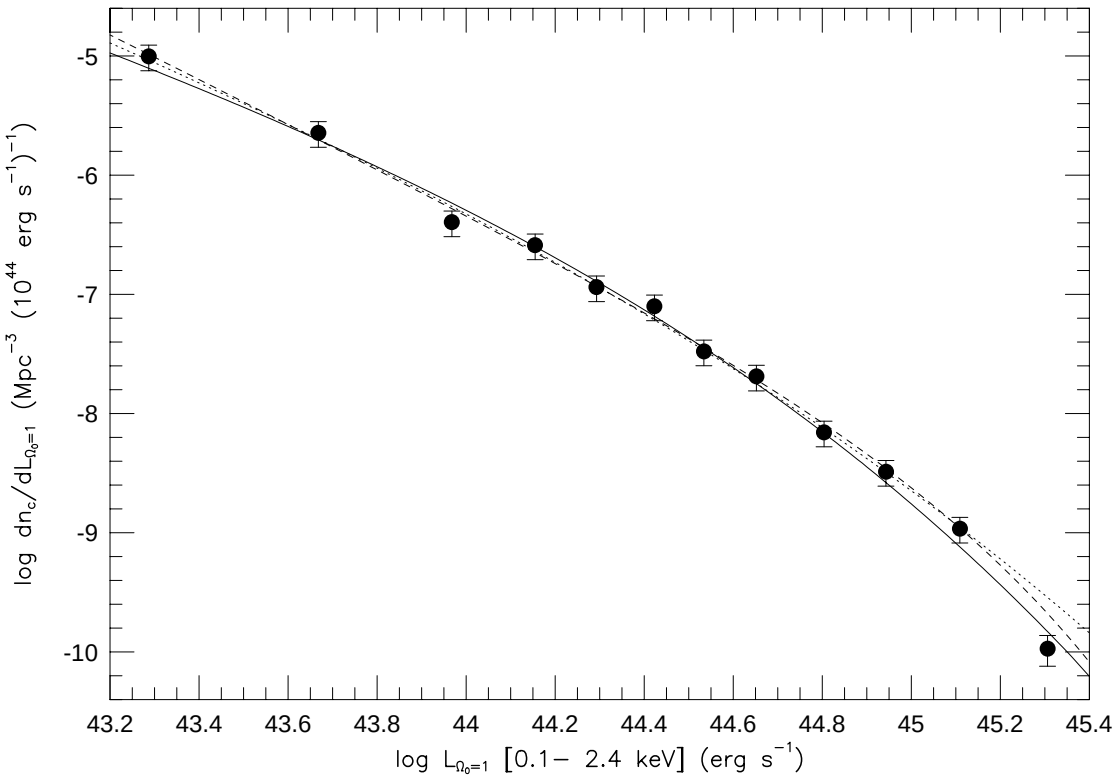

FIG. 2.—*ROSAT* BCS luminosity function of Ebeling et al. (1997). The solid line is the best fit of eq. (18) to all 12 luminosity bins. The dotted line is the best fit of eq. (18) to all but the highest luminosity bin (see § 3.2). The dashed line is the best-fit Schechter function of Ebeling et al. (1997).

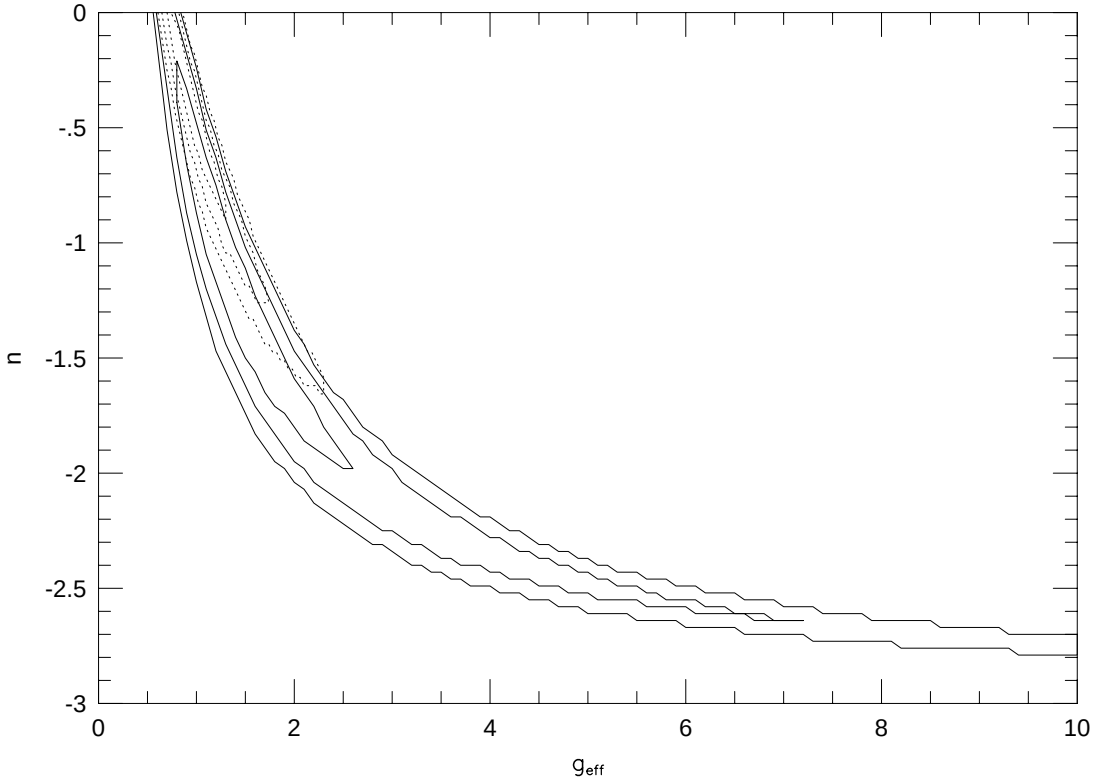

FIG. 3.—The 1, 2, and 3 σ credible regions of the posterior probability distributions of the fit of eq. (18) to all 12 luminosity bins (*dotted lines*) and all but the highest luminosity bin (*solid lines*) of the *ROSAT* BCS luminosity function (see § 3.2).

tion (17). This approximation is reasonable, unless the value of Ω_m is high, in which case one expects a lower comoving number density of X-ray clusters in the highest luminosity bins. This is because the highest luminosity bins more strongly sample the highest redshift BCS clusters than do the lower luminosity bins. Given this approximation—that $z = z_{\rm eff}$, a constant—equation (17) can only reproduce such a high-luminosity rollover of the luminosity function by favoring an artificially high value of n. To safeguard against this potential bias, we first fitted equation (17) to all 12 luminosity bins, then to all but the highest luminosity bin, then to all but the two highest luminosity bins, etc., until the fitted values of n and c do not change appreciably from fit to fit. Also, since Ebeling et al. (1997) have already corrected this luminosity function for sample completeness, we set $A(L_1, z_{\rm eff}) = 1$. Here, we ignore the dependence that this quantity has on Ω_m, which is a reasonable approximation since $z_{\rm eff} < 0.3$.

We find that only the highest luminosity bin noticeably changes our results. When we fit equation (17) to all 12 luminosity bins, we find that $n = -0.47^{+0.32}_{-0.31}$ and $g_{\rm eff} = 0.90^{+0.28}_{-0.14}$, where we have assumed a flat prior probability distribution in the range $-3 < n < 0$ and $0 < g_{\rm eff} < 10$, and the likelihood function is given by $e^{-\chi^2/2}$.[7] When we fit equation (17) to all but the highest luminosity bin, we find that $n = -1.83^{+0.85}_{-0.15}$ and $g_{\rm eff} = 1.20^{+0.70}_{-0.60}$. Ignoring additional high-luminosity bins does not appreciably change this result; consequently, in this paper, we use all but the highest luminosity bin to determine a constraint from the BCS. We will explore what this highest luminosity bin implies for the value of Ω_m in a later paper. In Figure 3, we plot the 1, 2, and 3 σ credible regions in the n-$g_{\rm eff}$ plane for both of the above fits. We do not plot credible regions in the n-c plane because, by equation (19), the parameter c is a degenerate function of the parameters $g_{\rm eff}$ and Ω_m (see § 3); however, credible regions in the n-c plane are easily recovered, given a value of Ω_m (see § 3.3). In Figure 2, we also plot the best-fit luminosity functions of these fits.

[7] See, e.g., Gregory & Loredo (1992) for an excellent discussion of Bayesian inference.

3.3. *The EMSS*

As described in § 3 the breadth of the luminosity and redshift ranges of the EMSS makes this catalog an ideal sample with which to probe Ω_m. In Figure 4, we plot the L_1-z distribution of the revised EMSS of Nichol et al. (1997), as well as the $z < 0.14$ portion of the original EMSS X-ray cluster subsample. The solid curves are contours of constant sampled differential volume, i.e., $A(L_1, z)dV(z)/dz = constant$. From left to right, these contours are equally spaced from zero (zero contour not shown). If the X-ray cluster luminosity function has not evolved over the redshift range of the EMSS, then at each luminosity, most of the observed X-ray clusters would be where most of the sampled differential volume is. This appears to be the case below $L_1 \sim 7 \times 10^{44}$ ergs s^{-1} (0.3–3.5 keV), which demonstrates agreement with the results of Collins et al. (1997), Nichol et al. (1997), Burke et al. (1997), Rosati et al. (1998), Jones et al. (1998), and Vikhlinin et al. (1998b), i.e., that the X-ray cluster luminosity function evolves only minimally, if at all, below $L_\star$ (see § 4). However, as was originally found by Gioia et al. (1990a; see also Henry et al. 1992), there appears to be a deficit of high-redshift X-ray clusters above $L_\star$. For example, given that six X-ray clusters were detected in the range

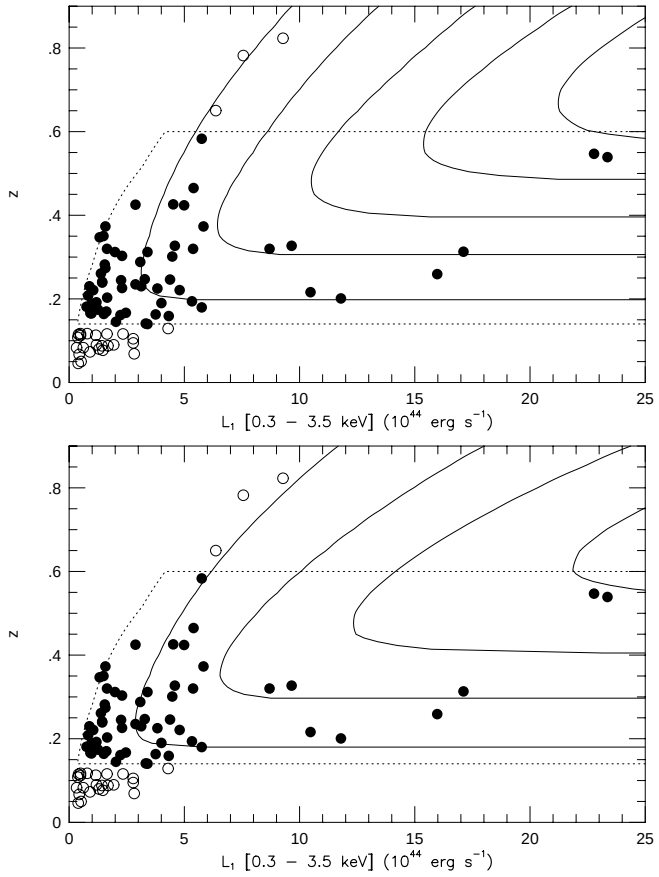

FIG. 4.—The L_1-z distribution of the EMSS clusters. From left to right, the solid curves are increasing, equally spaced (from zero, zero contour not shown) contours of constant sampled differential volume (see § 3.3). A deficit of high-redshift X-ray clusters is apparent above $L_1 \sim 7 \times 10^{44}$ ergs s^{-1}. The dotted curve is the more conservative of the two regions over which we fitted eq. (23) in § 3.3. Points interior to this region are solid. The top panel is for $\Omega_m = 0$, and the bottom panel is for $\Omega_m = 1$.

$0.14 < z < 0.4$ at $L_1 > 7 \times 10^{44}$ ergs s^{-1} (0.3–3.5 keV), one would expect $\sim$9 X-ray clusters in the range $0.4 < z < 0.6$ and $\sim$21 X-ray clusters between $0.4 < z < 0.9$ at these luminosities if the luminosity function were not evolving, yet only two and four clusters were detected in these redshift ranges, respectively. Hence, we find a factor of 4–5 fewer X-ray clusters at redshifts above $z = 0.4$ than below this redshift at these luminosities. This is only possible at the $\approx$1%–2% level with the no-evolution model. This suggests that high values of Ω_m may be favored (§ 3); however, we offer alternative interpretations of this deficit in § 4.

By Bayes' theorem, the posterior probability distribution for Ω_m, n, and c, $P(\Omega_m, n, c)$, is given by normalizing the product of the prior probability distribution and the likelihood function (e.g., Gregory & Loredo 1992). Here, we assume a flat prior probability distribution between $0 < \Omega_m < 1.5$, $-3 < n < 0$, and $0 < c < 3$. The likelihood function, $\mathscr{L}(\Omega_m, n, c)$, is given by (e.g., Cash 1979)

$$\mathscr{L}(\Omega_m, n, c) = \prod_{i=1}^{N_{\rm tot}} P(L_{1,i}, z_i \,|\, \Omega_m, n, c) \,, \qquad (28)$$

where $P(L_{1,i}, z_i \,|\, \Omega_m, n, c)$ is the probability that the ith X-ray cluster fits our model, given values of Ω_m, n, and c. For our model (eq. [22]), this probability is given by (e.g., Cash 1979)

$$P(L_1, z \,|\, \Omega_m, n, c) = \frac{A(L_1, z)}{N(L_l, L_u; z_l, z_u)} \frac{dV(z)}{dz} \frac{dn_c(L_1, z)}{dL_1} \,. \qquad (29)$$

Since both $dn_c(L_1, z)/dL_1$ and $N(L_l, L_u; z_l, z_u)$ are proportional to the normalization parameter a, our results are clearly independent of this parameter.

In equation (28), $N_{\rm tot}$ is the total number of X-ray clusters in the same region of the L_1-z plane as that over which $N(L_l, L_u; z_l, z_u)$ is defined. This region should be as broad as is reasonably possible, and it need not be rectangular, as the simple integration limits of equation (22) suggest. In this paper, we set $L_l < L_1 < L_u = 10^{45.5}$ ergs s^{-1}, where L_l is set by the limiting flux of the EMSS: $F(L_l, z) = 1.33 \times 10^{-13}$ ergs cm^{-2} s^{-1} (Henry et al. 1992); hence, L_l is a function of redshift.[8] Also in this paper, we set $0.14 = z_l < z < z_u = 0.6$. We exclude higher redshifts because (1) the L-T relation of Reichart et al. (1998) is derived from $z \lesssim 0.5$ X-ray clusters, so its accuracy should not be trusted at redshifts much in excess of this value and (2) optical identification becomes more difficult at these high redshifts (§ 1). This excludes three $\sim L_\star$ X-ray clusters, which reduces the total number of X-ray clusters in our sample from 64 to 61. Below, however, we repeat our analysis with $z_u = 0.9$ to show that the exclusion of these three X-ray clusters does not unfairly bias our results. In Figure 4, we mark this region of the L_1-z plane with a dotted line; solid points are interior to this region.

The posterior probability distribution for any two parameters, e.g., $P(\Omega_m, n)$, or one parameter, e.g., $P(\Omega_m)$, is given by marginalizing the posterior probability distribution for all three parameters, $P(\Omega_m, n, c)$, over the other parameters (e.g., Gregory & Loredo 1992). The 1, 2, and 3 σ credible regions are determined by integrating the posterior probability distribution over the most probable region of its parameter space until 68.3%, 95.4%, and 99.73% of this distribution has been integrated (e.g., Gregory & Loredo 1992). In Figure 5 we plot the 1, 2, and 3 σ credible regions of the two-dimensional posterior probability distributions $P(\Omega_m, n)$ (*top panel*) and $P(n, c)$ (*bottom panel*). The 1 σ credible intervals of the one-dimensional posterior probability distributions, i.e., $P(\Omega_m)$, $P(n)$, and $P(c)$, are $\Omega_m = 0.96^{+0.48}_{-0.38}$, $n = -2.28^{+0.36}_{-0.25}$, and $c = 0.66^{+0.48}_{-0.23}$. Hence, the EMSS favors high values of Ω_m and low values of n. Although these results by themselves are constraining $-\Omega_m < 0.2$, is ruled out at the 2.3 σ credible level; by combining the likelihood function of the EMSS with the posterior probability distribution of the BCS (Fig. 3), stronger constraints can be placed on these parameters.

We now determine the combined posterior probability distribution of the EMSS and the BCS. Let the likelihood function be that of the EMSS, as given by equation (28). However, instead of assuming a flat prior probability distribution for all three parameters, as we did above, only assume a flat prior probability distribution in the range $0 < \Omega_m < 1.5$ and use the posterior probability distribution of the $BCS - P_{\rm BCS}(n, g_{\rm eff})$ (Fig. 3), equation (19), and the

[8] In computing $L_l(z)$, we set $\Omega_m = 0$. This is because if we were to use a higher value of Ω_m when defining this curve, the selection function, $A(L_1, z)$, would be undefined for luminosities and redshifts near this curve when the value of Ω_m is lower than the curve-defining value (see eq. [21]).

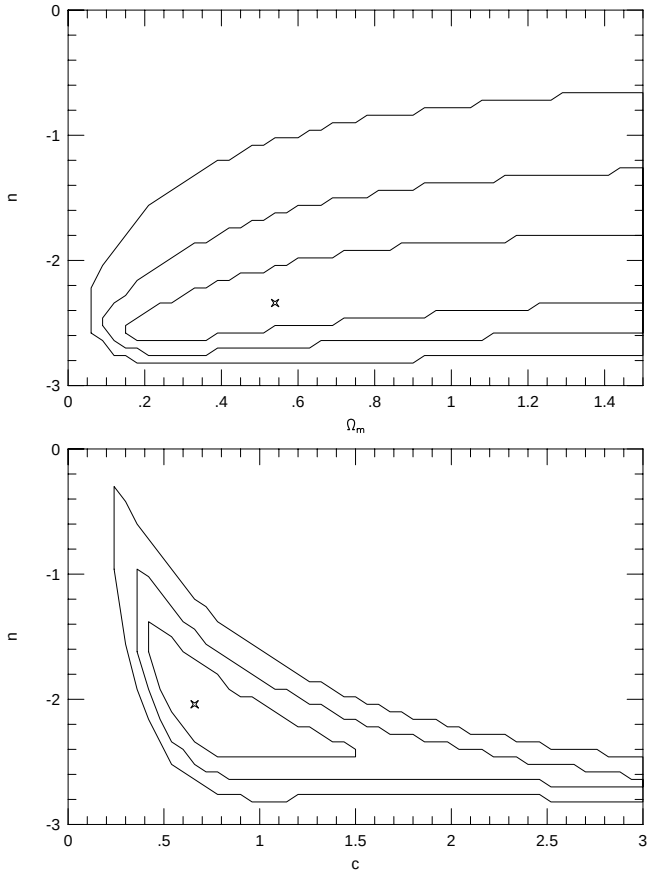

FIG. 5.—The 1, 2, and 3 σ credible regions of the marginalized posterior probability distributions $P(\Omega_m, n)$ (*top panel*) and $P(n, c)$ (*bottom panel*) of the fit of eq. (23) to the $0.14 < z < 0.6$ revised EMSS clusters (see § 3.3).

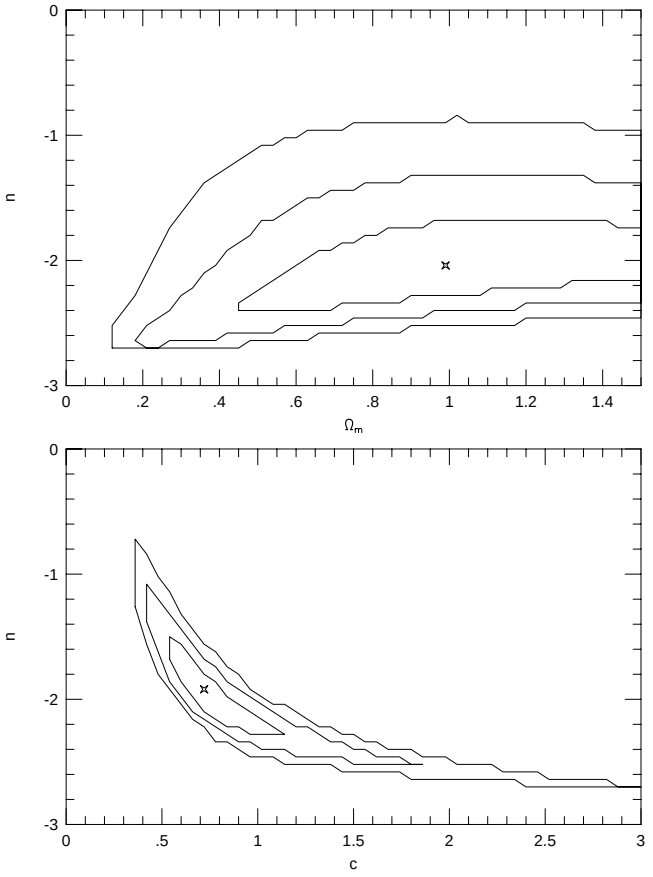

FIG. 6.—The 1, 2, and 3 σ credible regions of the marginalized posterior probability distributions $P(\Omega_m, n)$ (*top panel*) and $P(n, c)$ (*bottom panel*) of the fit of eq. (23) to the $0.14 < z < 0.6$ revised EMSS clusters and the *ROSAT* BCS luminosity function (see § 3.3).

effective redshift of the BCS, $z_{\rm eff} \sim 0.1$, to determine the full prior probability distribution: $P_{\rm BCS}(\Omega_m, n, c)$. In Figure 6 we plot credible regions of the two-dimensional combined EMSS/BCS posterior probability distributions $P(\Omega_m, n)$ and $P(n, c)$. In the three left-hand panels of Figure 8 we plot the one-dimensional combined EMSS/BCS posterior probability distributions. The dotted lines in this figure mark the 1, 2, and 3 σ credible intervals. We find that $\Omega_m = 0.96^{+0.36}_{-0.32}$, $n = -1.86^{+0.42}_{-0.34}$, and $c = 0.54^{+0.24}_{-0.12}$. Values of $\Omega_m < 0.2$ are ruled out at the 3.0 σ credible level.

To establish that the exclusion of the three $z > 0.6$, $\sim L_\star$ EMSS clusters does not unfairly bias our results, we repeat this analysis for $z_u = 0.9$. In Figure 7 we plot credible regions of the two-dimensional combined EMSS/BCS posterior probability distributions $P(\Omega_m, n)$ and $P(n, c)$. In the three right-hand panels of Figure 8 we plot the one-dimensional combined EMSS/BCS posterior probability distributions. In this case we find that $\Omega_m = 0.93^{+0.33}_{-0.26}$, $n = -1.50^{+0.37}_{-0.36}$, and $c = 0.48^{+0.12}_{-0.12}$. Values of $\Omega_m < 0.2$ are ruled out at the 3.5 σ credible level. Lower values of Ω_m are not favored for three reasons. First of all, it is clear from Figure 3 that we have added a great deal of volume for which there are no EMSS clusters above $L_\star$. Secondly, for the region of the L_1-z plane occupied by these three clusters, the EMSS surveyed roughly twice as much area if $\Omega_m = 1$ than it did if $\Omega_m = 0$ (§ 3). This is primarily because higher values of Ω_m imply lower luminosity distances, which imply higher fluxes for a given luminosity and, consequently, greater surveyed areas by equation (20). The third reason,

TABLE 1

FITTED VALUES OF THE X-RAY CLUSTER LUMINOSITY FUNCTION

Catalog(s)	z_u	s[a]	Ω_m	n	c	$P(\Omega_m > 0.2)$ (σ)
BCS[b]	...	...	...	$-1.83^{+0.85}_{-0.15}$	...	...
EMSS	0.6	$3.14 - 0.65\Omega_m$	$0.96^{+0.48}_{-0.38}$	$-2.28^{+0.36}_{-0.25}$	$0.66^{+0.48}_{-0.23}$	2.3
EMSS+BCS	0.6	$3.14 - 0.65\Omega_m$	$0.96^{+0.36}_{-0.32}$	$-1.86^{+0.42}_{-0.34}$	$0.54^{+0.24}_{-0.12}$	3.0
EMSS+BCS	0.9	$3.14 - 0.65\Omega_m$	$0.93^{+0.33}_{-0.26}$	$-1.50^{+0.37}_{-0.36}$	$0.48^{+0.12}_{-0.12}$	3.5
EMSS+BCS	0.6	$2.26 - 0.61\Omega_m$	$0.69^{+0.36}_{-0.27}$	$-1.74^{+0.42}_{-0.36}$	$0.48^{+0.28}_{-0.12}$	2.6
EMSS+BCS	0.6	$3.79 - 0.59\Omega_m$	$1.17^{+0.33}_{-0.28}$	$-1.98^{+0.34}_{-0.30}$	$0.66^{+0.25}_{-0.18}$	3.2

[a] Reichart et al. 1998.
[b] $g_{\rm eff} = 1.20^{+0.70}_{-0.60}$.

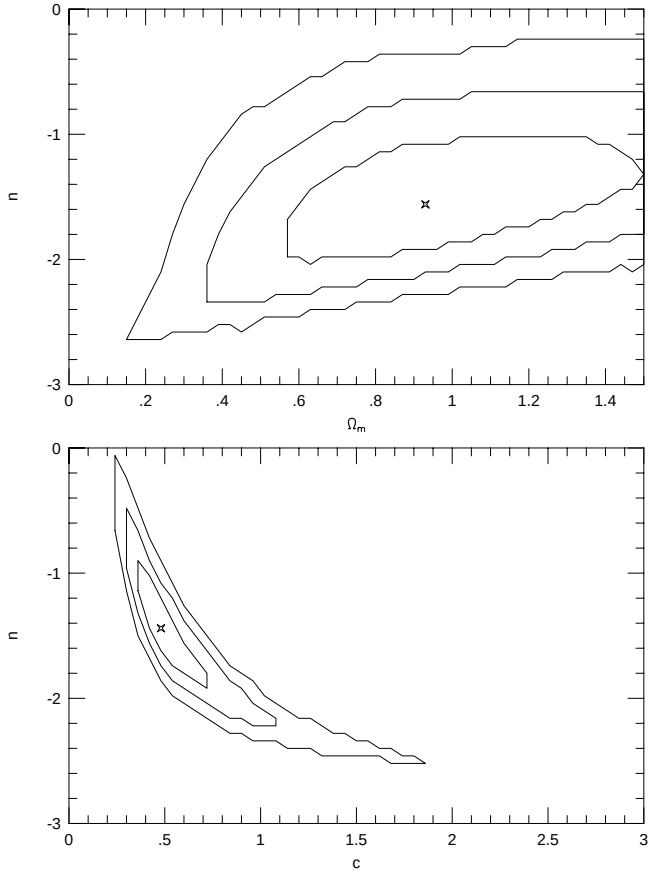

FIG. 7.—The 1, 2, and 3 σ credible regions of the marginalized posterior probability distributions $P(\Omega_m, n)$ (*top panel*) and $P(n, c)$ (*bottom panel*) of the fit of eq. (23) to the $0.14 < z < 0.9$ revised EMSS clusters and the *ROSAT* BCS luminosity function (see § 3.3).

also mentioned in § 3, is that at luminosities $\lesssim L_\star$, the luminosity function itself is a nonnegligible, increasing function of Ω_m. At these luminosities, the redshift dependence of the luminosity function is dominated by the function $f(z)$. This function is approximately given by (eqs. [18], [2], and [16])

$$f(z) \propto \begin{cases} (1+z)^{0.33(3-n)} & (\Omega_m = 0) \\ (1+z)^{1+0.23(3-n)} & (\Omega_m = 1)\ . \end{cases} \tag{30}$$

Consequently, there is an additional factor of $\approx(1+z)^{1/2}$ in the $\Omega_m = 1$ case. Although our $z_u = 0.9$ results are more constraining than are our $z_u = 0.6$ results, for the reasons stated above, we feel less confident about these results than we do about our $z_u = 0.6$ results.

We now show that the uncertainty in the value of s does not significantly affect our results. In the three left-hand panels of Figure 9, we plot the one-dimensional combined EMSS/BCS posterior probability distributions, once again for $z_u = 0.6$, except that we have now used the $-1\ \sigma$ value of s from Reichart et al. (1998). In the three right-hand panels of Figure 9, we plot the same distributions, but for the $+1\ \sigma$ value of s from Reichart et al. (1998). The effect of varying the value of s by $\pm 1\ \sigma$ is a variation in the values of the fitted parameters by less than the extent of their $\pm 1\ \sigma$ uncertainties. If we add these uncertainties in quadrature, we find that $\Omega_m \approx 1.0 \pm 0.4$, $n \approx -1.9 \pm 0.4$, and $c \approx 0.55^{+0.25}_{-0.15}$. One-dimensional credible intervals for all of the fitted values in this section are compiled in Table 1.

4. DISCUSSION AND CONCLUSIONS

In this paper we have constructed from the Press-Schechter mass function and the empirical X-ray cluster L-T relation of Reichart et al. (1998) an X-ray cluster luminosity function that can be applied to the growing number of independent, high-redshift, X-ray cluster luminosity catalogs to constrain cosmological parameters. In particular, we have incorporated the evolution of the L-T relation and all significant dependences on Ω_m of the luminosity and selection functions into our Bayesian inference analysis. For a fixed value of H_0, we have applied this luminosity function to broad subsets of the revised EMSS X-ray cluster subsample of Nichol et al. (1997) and to the *ROSAT* BCS luminosity function of Ebeling et al. (1997) to constrain Ω_m. For the 61 revised EMSS clusters in the range $0.14 < z < 0.6$, we find that $\Omega_m = 0.96^{+0.36}_{-0.32}$ and $n = -1.86^{+0.42}_{-0.34}$; for all 64 revised EMSS clusters in the range $0.14 < z < 0.9$, we find that $\Omega_m = 0.93^{+0.33}_{-0.26}$ and $n = -1.50^{+0.37}_{-0.36}$. These high values of Ω_m are the result of an apparent deficit of high-redshift, luminous X-ray clusters, which suggests that the X-ray cluster luminosity function has evolved above $L_\star$.

Nichol et al. (1997) suggested that the statistical evidence for the evolution of the EMSS luminosity function was only minimal. At first glance, this appears to be in contradiction to one of the conclusions of this paper. However, since Nichol et al. (1997) used a power-law luminosity function—which they did for purposes of comparison with the original EMSS result of Henry et al. (1992)—instead of a luminosity function that permits different degrees of evolution below and above $L_\star$, as we have done in this paper, their results are most directly applicable below $L_\star$: this is the luminosity range of the vast majority of the EMSS clusters, so it is by this luminosity range that their results have most strongly been weighted. The fact that the X-ray cluster luminosity function does not evolve below $L_\star$ has since been shown by Collins et al. (1997), Burke et al. (1997), Rosati et al. (1998), Jones et al. (1998), and Vikhlinin et al. (1998b). That the luminosity function appears to evolve above $L_\star$ is in agreement with the original EMSS findings of Gioia et al. (1990a), as well as the findings of Vikhlinin et al. (1998b, 1998a) with the 160 deg^2 survey.

The value of Ω_m that we find that this high-luminosity evolution in the EMSS corresponds to is consistent with the values found by Sadat, Blanchard, & Oukbir (1998) ($\Omega_m = 0.85 \pm 0.2$) and Blanchard & Bartlett (1998) ($\Omega_m \approx 1$), based on the work of Oukbir & Blanchard (1992, 1997). Our value of Ω_m is somewhat consistent with the values found by Henry (1997) ($\Omega_m = 0.50 \pm 0.14$) and Eke et al. (1998) ($\Omega_m = 0.45 \pm 0.2$); however, Viana & Liddle (1998) have performed a more extensive error analysis on a conservative subset of the data of these authors and find that $\Omega_m \sim 0.75$ with $\Omega_m > 0.3$ at the 90% confidence level and $\Omega_m \sim 1$ still viable. Blanchard et al. (1998) find almost identical results ($\Omega_m \sim 0.74$, with $0.3 < \Omega_m < 1.2$ at the 95% confidence level) from these data. Finally, our value of Ω_m is inconsistent with the values found by Bahcall, Fan, & Cen (1997) ($\Omega_m = 0.3 \pm 0.1$), Fan, Bahcall, & Cen (1997) ($\Omega_m \approx 0.3 \pm 0.1$), and Bahcall & Fan (1998) ($\Omega_m = 0.2^{+0.3}_{-0.1}$).

Our value of n is consistent with the values found by Henry & Arnaud (1991) ($n = -1.7^{+0.65}_{-0.35}$) and Henry et al. (1992) ($n = -2.10^{+0.27}_{-0.15}$), where these authors set $\Omega_m = 1$. Our value of n is also consistent with the value found by

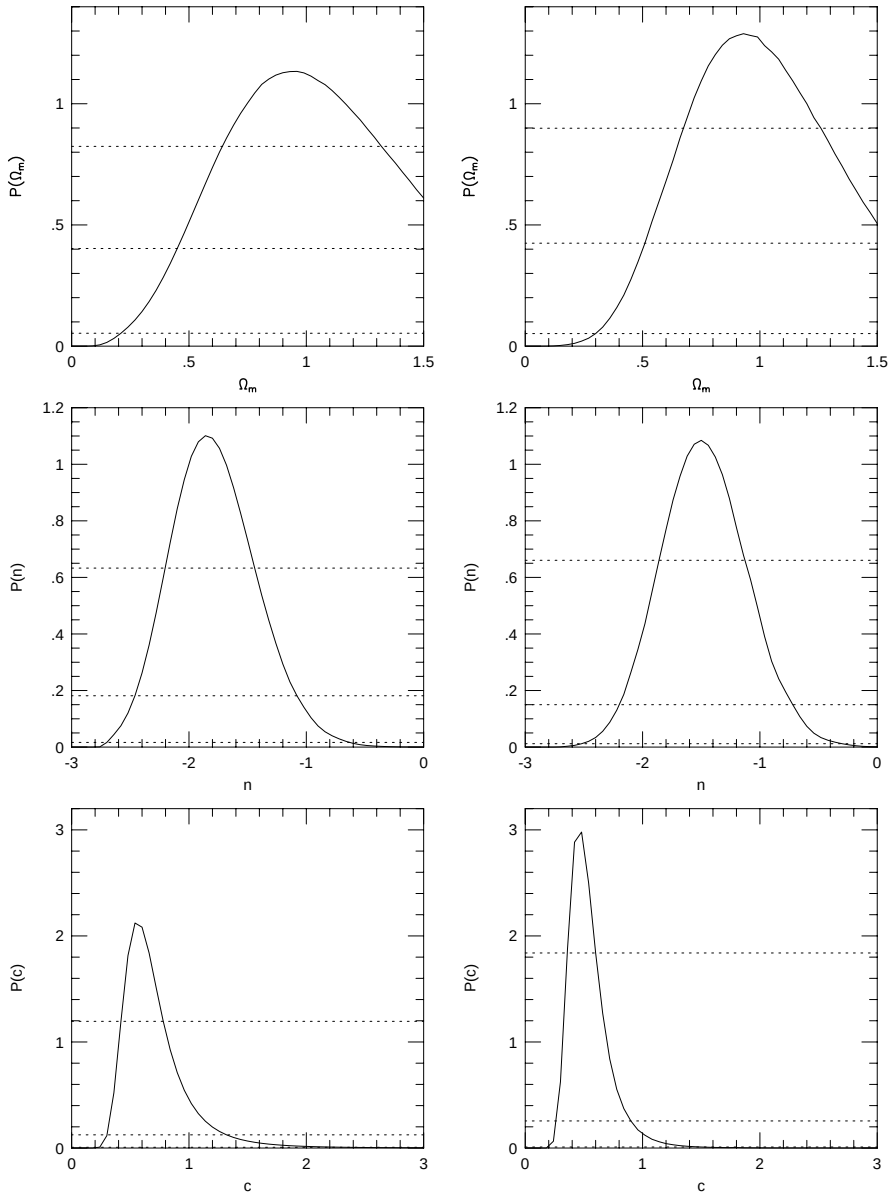

FIG. 8.—Marginalized posterior probability distributions $P(\Omega_m)$, $P(n)$, and $P(c)$ of the fit of eq. (23) to the $0.14 < z < z_u$ revised EMSS clusters and the *ROSAT* BCS luminosity function. For the three left panels, $z_u = 0.6$; for the three right panels, $z_u = 0.9$. The dotted lines mark the 1, 2, and 3 σ credible intervals (see § 3.3).

Eke et al. (1998) ($n = -1.69^{+0.12}_{-0.07}$), where these authors included Ω_m as a free parameter. Our value of n is somewhat consistent with the value that Bahcall et al. (1997), Fan et al. (1997), and Bahcall & Fan (1998) adopted ($n = -1.4$).

Taken as an ensemble, these results are perhaps discouraging in that they span the entire range of acceptable solutions: $0.2 \lesssim \Omega_m \lesssim 1$. This suggests that as yet unknown systematic effects may be plaguing some, if not all, of these results. We briefly identify seven areas where systematic effects could enter our and similar analyses. (1) The first is the Press-Schechter mass function itself; however, numerical simulations (e.g., Eke et al. 1996; Bryan & Norman 1997; Borgani et al. 1998) consistently show that the Press-Schechter mass function is an adequate approximation. (2) The spherical collapse model of cluster formation (eqs. [2] and [26]) may be inadequate. For example, numerical simulations by Governato et al. (1998) suggest that in equation (26), the expression $1.69(1 + z)$ may really be as low as $\sim 1.6(1 + z)^{0.9}$. This suggests that use of the spherical collapse model may lead to underestimated values of Ω_m; however, this is only a $\lesssim 10\%$ effect. (3) Technically, equation (10) only holds when $\Omega_m = 1$. Recently, Voit & Donahue (1998) derived a virial theorem that holds for all values of Ω_m and that allows for the fact that clusters grow gradually; their mass-temperature (M-T) relation reduces to equation (10) when $\Omega_m = 1$. We find that M-T relations with functional forms that are similar to that of the M-T relation of Voit & Donahue (1998) reduce our fitted value of Ω_m by $\lesssim 10\%$; however, further investigation and use of this M-T relation is clearly needed. (4) Also on the subject of the M-T relation, care must be taken when fitting to X-ray cluster temperature catalogs: cooling flows lower the measured temperature of most X-ray clusters, which should systematically affect values of Ω_m that are determined in this way. (5) Based on the cooling flow–corrected X-ray cluster temperature catalogs of Markevitch (1998) and Allen &

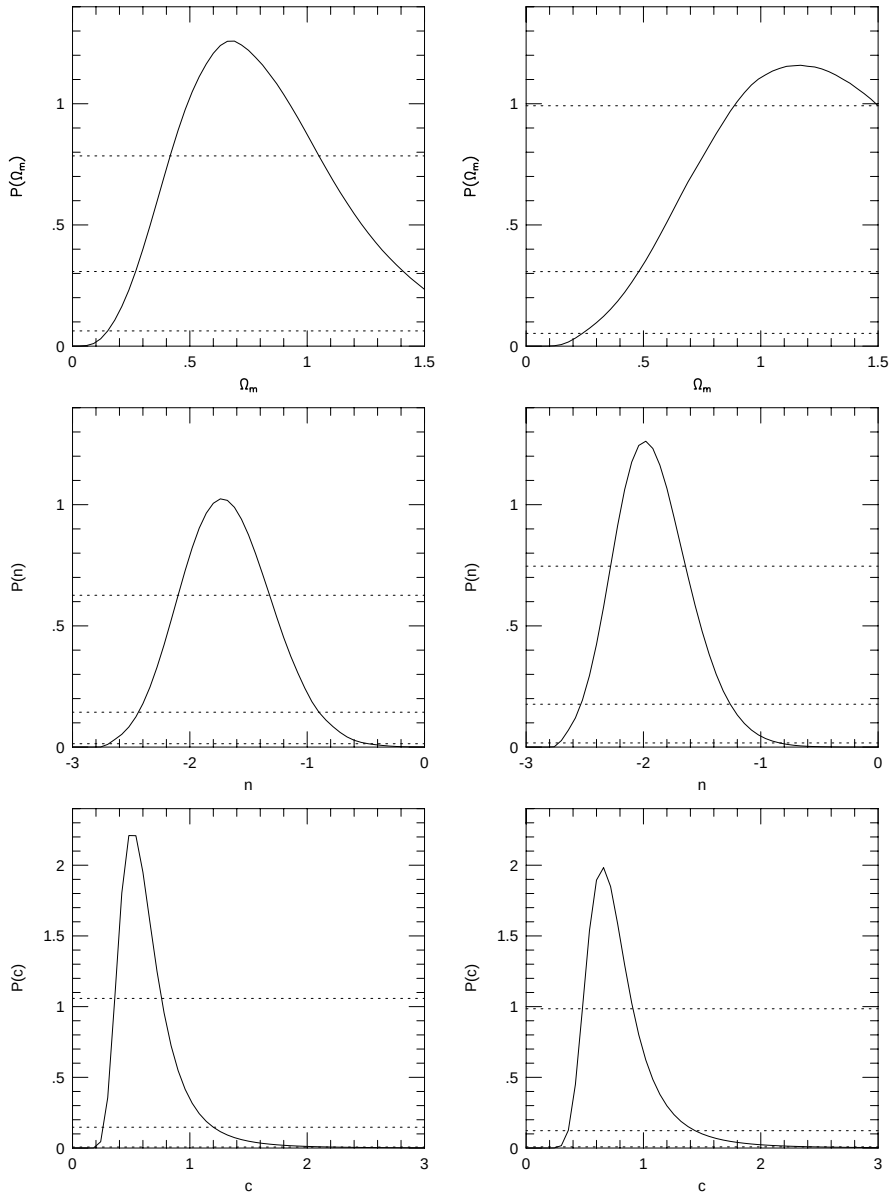

FIG. 9.—Marginalized posterior probability distributions $P(\Omega_m)$, $P(n)$, and $P(c)$ of the fit of eq. (23) to the $0.14 < z < 0.6$ revised EMSS clusters and the *ROSAT* BCS luminosity function. For the three left panels, we use the $-1\ \sigma$ value of s from Reichart et al. (1998); for the three right panels, we use the $+1\ \sigma$ value of s from Reichart et al. (1998). The dotted lines mark the 1, 2, and 3 σ credible intervals (see § 3.3).

Fabian (1998), Reichart et al. (1998) determined an empirical L-T relation between measured luminosities and cooling flow–corrected temperatures that holds for $z \lesssim 0.5$ and for luminosities that are typical of X-ray cluster catalogs (see § 3.1); however, more cooling flow–corrected X-ray cluster temperature measurements are needed to determine what, if any, exceptions exist to this L-T relation and to extend it to higher redshifts. (6) The art of determining an X-ray cluster catalog's selection function is a constantly improving science; modern selection functions are determined via extensive numerical simulations. An alternative explanation to our high-Ω_m result is that the EMSS, for whatever reasons, missed many high-redshift, high-luminosity X-ray clusters beyond what is accounted for by their selection function (see § 3.3). However, given that the EMSS detected many high-redshift, low-luminosity X-ray clusters, this seems to be an unlikely scenario. (7) Finally, our cosmological model may be inadequate. We did not investigate the effects of a cosmological constant in this paper; however, many authors have demonstrated that the inclusion of a cosmological constant has little effect on the determined value of Ω_m (see § 1). Also, the effects of quintessent and other exotic cosmologies have not yet been investigated in this context.

Some of these potential sources of systematic error can be safeguarded against. For example, the spherical collapse model, the M-T relation, and the L-T relation all have proportionality factors that are potential sources of systematic error. However, as we have shown in § 2.1, all of these factors, as well as the parameter σ_8, group together, giving us our parameter c. Since we fit for c, these factors cannot bias our result. However, inadequate functional forms for these relations, as well as for the other functions listed above, can bias our results and others' results.

In addition to further theoretical and numerical development of this formalism, only the continued construction of X-ray cluster catalogs will act to further resolve these issues. Fortunately, the number of X-ray cluster luminosity catalogs is growing rapidly. One such catalog is the Southern SHARC (Collins et al. 1997; Burke et al. 1997). The redshift and luminosity ranges of the Southern SHARC are $z < 0.7$ and $L_1 < 3 \times 10^{44}$ ergs s^{-1} (0.5–2.0 keV). Although the Southern SHARC does not span the luminosity range of the EMSS, it will provide a good consistency check of our EMSS results. Our analysis of this catalog is underway.

Two similar X-ray cluster catalogs that can serve a similar purpose are the *ROSAT* Deep Cluster Survey (RDCS) (Rosati et al. 1998) and the Wide Angle *ROSAT* Pointed Survey (WARPS) (Jones et al. 1998). The RDCS spans the redshift and luminosity ranges $z < 0.8$ and $L_1 < 3 \times 10^{44}$ ergs s^{-1} (0.5–2.0 keV). The WARPS spans the redshift and luminosity ranges $z < 0.7$ and $L_1 < 2 \times 10^{44}$ ergs s^{-1} (0.5–2.0 keV). An analysis of the RDCS is also underway (Borgani et al. 1998).

The 160 deg^2 survey (Vikhlinin et al. 1998a) and the Bright SHARC (Romer et al. 1998), a high-luminosity extension of the Southern SHARC that is currently under construction, span redshift and luminosity ranges that rival those of the EMSS. Consequently, these catalogs will provide strong, independent checks of the EMSS results.

Finally, local ($z_{\rm eff} \sim 0.1$) X-ray cluster catalogs, such as the *ROSAT* BCS, are of great importance. Although these samples do not have the redshift leverage to constrain cosmological parameters, their large sizes make them excellent samples to better constrain the parameters n and c. Samples like the EMSS, the 160 deg^2 survey, and the Bright SHARC do not have sufficient luminosity leverage to strongly constrain these parameters, which leads to weaker constraints on the cosmological parameters. However, a simultaneous analysis of a local X-ray cluster catalog—as opposed to a local X-ray cluster luminosity function as we have used in this paper—and any of these high-redshift, high-luminosity X-ray cluster catalogs could lead to significantly improved constraints on all of these parameters.

This research has been partially funded by NASA grants NAG5-6548 and NAG5-2432. We are very grateful to H. Ebeling for providing us with the data for Figure 2. Also, we are grateful to A. Blanchard, S. Borgani, C. Graziani, D. Q. Lamb, C. A. Metzler, C. Scharf, M. S. Turner, and J. M. Quashnock for valuable discussions. We are also very grateful to our anonymous referee, whose input has greatly improved this paper. D. E. R. is especially grateful to Dr. and Mrs. Bernard Keisler for their hospitality during the summers of 1997 and 1998.

REFERENCES

Allen, S. W., & Fabian, A. C. 1998, MNRAS, 297, L57
Arnaud, M., & Evrard, A. E. 1998, MNRAS, in press
Avni, Y., & Bahcall, J. N. 1980, ApJ, 235, 694
Bahcall, N. A., & Fan, X. 1998, ApJ, 504, 1
Bahcall, N. A., Fan, X., & Cen, R. 1997, ApJ, 485, L53
Blanchard, A., & Bartlett, J. G. 1997, A&A, 332, L49
Blanchard, A., Bartlett, J. G., & Sadat, R. 1998, in Les Comptes Rendus de l'Academie des Sciences, in press
Borgani, S., Rosati, P., Tozzi, P., & Norman, C. 1998, ApJ, in press
Bryan, G. L., & Norman, M. L. 1998, ApJ, 495, 80
Burke, D. J., Collins, C. A., Sharples, R. M., Romer, A. K., Holden, B. P., & Nichol, R. C. 1997, ApJ, 488, L83
Cash, A. 1979, ApJ, 228, 939
Collins, C. A., Burke, D. J., Romer, A. K., Sharples, R. M., & Nichol, R. C. 1997, ApJ, 479, L117
David, L. P., Slyz, A., Jones, C., Forman, W., Vrtilek, S. D., & Arnaud, K. A. 1993, ApJ, 412, 479
Ebeling, H., Edge, A. C., Fabian, A. C., Allen, S. W., Crawford, C. S., & Böehringer, H. 1997, ApJ, 479, L101
Edge, A. C., & Stewart, G. C. 1991, MNRAS, 252, 414
Eke, V. R., Cole, S., Frenk, C. S., & Henry, J. P. 1998, MNRAS, 298, 1145
Eke, V. R., Cole, S., Frenk, C. S., & Navarro, J. F. 1996, MNRAS, 281, 703
Evrard, A. E., & Henry, J. P. 1991, ApJ, 383, 95
Fan, X., Bahcall, N. A., & Cen, R. 1997, ApJ, 490, L123
Gioia, I. M., Henry, J. P., Maccacaro, T., Morris, S. L., Stocke, J. T., & Wolter, A. 1990a, ApJ, 356, L35
Gioia, I. M., & Luppino, G. A. 1995, ApJS, 94, 583
Gioia, I. M., Maccacaro, T., Schild, R. E., Wolter, A., Stocke, J. T., Morris, S. L., & Henry, J. P. 1990b, ApJS, 72, 567
Governato, F., Babul, A., Quinn, T., Tozzi, P., Baugh, C. M., Katz, N., & Lake, G. 1998, MNRAS, submitted (astro-ph 9810189)
Gregory, P. C., & Loredo, T. J. 1992, ApJ, 398, 146
Henry, J. P. 1997, ApJ, 489, L1
Henry, J. P., & Arnaud, K. A. 1991, ApJ, 372, 410
Henry, J. P., Gioia, I. M., Maccacaro, T., Morris, S. L., Stocke, J. T., & Wolter, A. 1992, ApJ, 386, 408
Jones, L. R., Scharf, C., Ebeling, H., Perlman, E., Wegner, G., Malkan, M., & Horner, D. 1998, ApJ, 495, 100
Kaiser, N. 1986, MNRAS, 222, 323
———. 1991, ApJ, 383, 104
Lacey, C., & Cole, S. 1993, MNRAS, 262, 627
Markevitch, M. 1998, ApJ, 504, 27
Mathiesen, B., & Evrard, A. E. 1998, MNRAS, 295, 769
Mushotzky, R. F., & Scharf, C. A. 1997, ApJ, 482, L13
Nichol, R. C., Holden, B. P., Romer, A. K., Ulmer, M. P., Burke, D. J., & Collins, C. A. 1997, ApJ, 481, 644
Oukbir, J., & Blanchard, A. 1992, A&A, 262, L21
———. 1997, A&A, 317, 10
Peebles, P. J. E. 1980, The Large Scale Structure of the Universe (Princeton: Princeton Univ. Press)
Press, W. H., & Schechter, P. 1974, ApJ, 187, 425
Reichart, D. E., Castander, F. J., & Nichol, R. C. 1999, ApJ, 516, 8
Romer, A. K., Nichol, R. C., Collins, C. A., Burke, D. J., Holden, B. P., Ulmer, M. P., Pildis, R. A., & Metevier, A. 1998, Astron. Nachr, 319, 83
Rosati, P., Della Ceca, R., Norman, C., & Giacconi, R. 1998, ApJ, 492, L21
Sadat, R., Blanchard, A., & Oukbir, J. 1998, A&A, 329, 21
Stocke, J. T., Morris, S. L., Gioia, I. M., Maccacaro, T., Schild, R., Wolter, A., Fleming, T. A., & Henry, J. P. 1991, ApJS, 76, 813
Viana, P. T. P., & Liddle, A. R. 1998, MNRAS, 303, 535
Vikhlinin, A., McNamara, B. R., Forman, W., & Jones, C. 1998a, ApJ, 502, 558
Vikhlinin, A., McNamara, B. R., Forman, W., Jones, C., Quintana, H., & Hornstrup, A. 1998b, ApJ, 498, L21
Voit, G. M., & Donahue, M. 1998, ApJ, 500, L111